Endothelial $\alpha_v\beta_3$ Integrin–Targeted Fumagillin Nanoparticles Inhibit Angiogenesis in Atherosclerosis

Patrick M. Winter, Anne M. Neubauer, Shelton D. Caruthers, Thomas D. Harris, J. David Robertson, Todd A. Williams, Anne H. Schmieder, Grace Hu, John S. Allen, Elizabeth K. Lacy, Samuel A. Wickline, Gregory M. Lanza

Objective—Angiogenic expansion of the vasa vasorum is a well-known feature of progressive atherosclerosis, suggesting that antiangiogenic therapies may stabilize or regress plaques. $\alpha_v\beta_3$ Integrin–targeted paramagnetic nanoparticles were prepared for noninvasive assessment of angiogenesis in early atherosclerosis, for site-specific delivery of antiangiogenic drug, and for quantitative follow-up of response.

Methods and Results—Expression of $\alpha_v\beta_3$ integrin by vasa vasorum was imaged at 1.5 T in cholesterol-fed rabbit aortas using integrin-targeted paramagnetic nanoparticles that incorporated fumagillin at 0 μg/kg or 30 μg/kg. Both formulations produced similar MRI signal enhancement (16.7%±1.1%) when integrated across all aortic slices from the renal arteries to the diaphragm. Seven days after this single treatment, integrin-targeted paramagnetic nanoparticles were readministered and showed decreased MRI enhancement among fumagillin-treated rabbits (2.9%±1.6%) but not in untreated rabbits (18.1%±2.1%). In a third group of rabbits, nontargeted fumagillin nanoparticles did not alter vascular $\alpha_v\beta_3$-integrin expression (12.4%±0.9%; $P>0.05$) versus the no-drug control. In a second study focused on microscopic changes, fewer microvessels in the fumagillin-treated rabbit aorta were counted compared with control rabbits.

Conclusions—This study illustrates the potential of combined molecular imaging and drug delivery with targeted nanoparticles to noninvasively define atherosclerotic burden, to deliver effective targeted drug at a fraction of previous levels, and to quantify local response to treatment. (***Arterioscler Thromb Vasc Biol.* 2006;25:000-000.)**

Key Words: magnetic resonance imaging ■ atherosclerosis ■ molecular imaging ■ angiogenesis ■ nanoparticles ■ fumagillin

A key feature of the atherosclerotic process is the angiogenic expansion of the vasa vasorum in the adventitia, which extends into the thickening intimal layer of the atheroma in concert with other neovessels originating from the primary arterial lumen.[1] Extensive neovascular proliferation within atherosclerotic plaques is prominent within "culprit" lesions clinically associated with unstable angina, myocardial infarction, and stroke.[2–4] Plaque angiogenesis has been suggested to promote plaque growth, intraplaque hemorrhage,[5] and lesion instability.

Magnetic resonance (MR) molecular imaging of focal angiogenesis in vivo with integrin-targeted paramagnetic contrast agents was reported with perfluorocarbon nanoparticles[6–8] and liposomes.[9] Subsequently, we have developed MRI and postprocessing techniques to permit molecular imaging of the diffuse proliferating neovasculature associated with atherosclerotic plaque development.[10,11] The widespread expression of $\alpha_v\beta_3$ integrins observed by MR agreed with the diffuse nature of angiogenesis microscopically observed in the early atherosclerotic aortas of cholesterol-fed rabbits.

The importance of angiogenesis in the progression of atherosclerotic plaque combined with the antiangiogenic impact of 3-hydroxy-3-methylglutaryl (HMG)–coenzyme A (CoA) reductase inhibitors,[12] suggests that suppression of vasa vasorum expansion could stabilize or reverse disease progression. Antiangiogenic agents have been shown to decrease both neovascular proliferation and plaque development in animal models of atherosclerosis when administered chronically at high dosages.[13] However, chronic high doses of TNP-470, a water soluble form of fumagillin, is associated with significant neurocognitive adverse effects in humans.[14,15]

Targeted perfluorocarbon nanoparticles can specifically deposit lipophilic agents such as doxorubicin or paclitaxel into the cell membrane and inhibit the proliferation of vascular smooth muscle cells in vitro.[16] In the present study, the concept of combined imaging and delivery of fumagillin with $\alpha_v\beta_3$ integrin–targeted paramagnetic nanoparticles is explored as a tool toward quantifying angiogenesis and

Original received August 18, 2005; final version accepted June 23, 2006.

From the Department of Medicine (P.M.W., A.M.N., S.D.C., T.A.W., A.H.S., G.H., J.S.A., E.K.L., S.A.W., G.M.L.), Cardiovascular Magnetic Resonance Laboratories, Washington University School of Medicine, St Louis, Mo; Philips Medical Systems (S.D.C.), Cleveland, Ohio; Bristol-Myers Squibb Medical Imaging (T.D.H.), Billerica, Mass; and the University of Missouri Research Reactor (J.D.R.), Columbia.

Correspondence to Patrick M. Winter, PhD, Department of Medicine, Washington University, 660 S Euclid Ave, Campus Box 8086, St Louis, MO 63110. E-mail patrick@cvu.wustl.edu

Arterioscler Thromb Vasc Biol. **is available at http://www.atvbaha.org** **DOI: 10.1161/01.ATV.0000235724.11299.76**

inhibiting the proliferation of the vasa vasorum in hyperlipidemic rabbits. The objectives were: (1) noninvasive detection and spatial delineation of $\alpha_v\beta_3$-integrin expression as a marker of aortic plaque angiogenesis at clinically relevant field strengths; (2) local delivery of an effective, single treatment of fumagillin to inhibit plaque angiogenesis at a dosage several orders of magnitude lower than previously reported; and (3) noninvasive follow-up assessment of the effect of targeted fumagillin delivery on aortic neovascularity.

Methods

Nanoparticle Formulations

Paramagnetic perfluorocarbon nanoparticles targeted to $\alpha_v\beta_3$ integrins were prepared analogous to previous reports.[11] In general, the emulsions comprised 20% (vol/vol) perfluorooctylbromide (PFO) (Minnesota Manufacturing and Mining), 2% (wt/vol) of a surfactant comixture, 1.7% (wt/vol) glycerin, and water for the balance. The surfactant comixture included 68 mole% lecithin (Avanti Polar Lipids Inc), 0.1 mole% peptidomimetic vitronectin antagonist (US Patent 6,322,770)[17–19] conjugated to polyethylene glycol $(PEG)_{2000}$-phosphatidylethanolamine (Avanti Polar Lipids Inc), 1.8 mole% phosphatidylethanolamine (Avanti Polar Lipids Inc), and 30 mole% gadolinium diethylene-triamine-pentaacetic acid-bis-oleate (Gateway Chemical Technologies) in chloroform:methanol (3:1), which was dried to a lipid film under vacuum. Therapeutic nanoparticle formulations included 0.2 mole% fumagillin (a gift from the National Cancer Institute), which was added to the surfactant mixture at the proportionate expense of lecithin. Nontargeted nanoparticles excluded the integrin-homing ligand, which was replaced in the surfactant mixture by an equivalent increase in dipalmitoyl phosphatidylethanolamine.

The surfactant components were prepared as published elsewhere,[11,16,20] combined with PFOB and distilled deionized water, and emulsified (Microfluidics Inc) at 20 000 psi for 4 minutes. Particle sizes were determined at 37°C with a laser light scattering submicron particle analyzer (Malvern Instruments). The concentrations of Gd^{3+} and nanoparticles in the emulsion were measured and the number of Gd^{3+}-complexes per nanoparticle was calculated as described previously.[21] Bioactivity of the $\alpha_v\beta_3$ integrin–targeted nanoparticles was confirmed using an in vitro vitronectin cell adhesion assay previously described[7] before use in animals.

Fumagillin Dissolution

Fumagillin nanoparticle emulsions (250 μL) were dialyzed in 60 000 molecular weight cutoff dialysis tubing against 3.5 mL of releasing medium (0.9% NaCl, 0.2 mg/mL human serum albumin, and 0.05% sodium azide) and continuously agitated at 37°C. The releasing medium was replaced daily and analyzed for fumagillin concentration. Fumagillin was analyzed by reverse-phase high-performance liquid chromatography (HPLC) (Waters Corporation) using a Waters Novapak C_{18}, 60 Å, 4-μm reversed-phase column (3.9×150 mm) with an isocratic 50% acetonitrile/0.05% phosphoric acid mobile phase (1 mL/min at ambient temperature).

MRI Protocol and Analysis

The experimental protocol was approved by the Animal Studies Committee of the Washington University School of Medicine. Male New Zealand White rabbits (Charles River Laboratories) were fed a 0.5% cholesterol diet (Purina Mills) for ≈80 days. In contradistinction to our previous study with this model,[11] the cholesterol component of the diet was reduced from 1.0% to 0.5%, which reduced the severity of atherosclerotic plaque formation in the aorta but improved the health of the animals in the study.

At the conclusion of the 80-day diet, all animals were anesthetized with 1% to 2% isoflurane and imaged by MRI using a 1.5 T clinical scanner (NT Intera CV, Philips Medical Systems) and a quadrature birdcage radiofrequency receive coil. Immediately following the MRI, rabbits were injected via the ear vein with $\alpha_v\beta_3$-targeted fumagillin nanoparticles (n=5), $\alpha_v\beta_3$-targeted nanoparticles without fumagillin (n=6), or nontargeted fumagillin nanoparticles (n=6) at 1.0 mL/kg. Four hours after nanoparticle injection, rabbits were reimaged to assess the magnitude and distribution of signal enhancement. Multislice, T_1-weighted, spin-echo, fat-suppressed, black-blood images were acquired of the entire abdominal aorta from the diaphragm to 5 cm past the renal arteries (TR=380 ms, TE=11 ms, 250×250 μm in-plane resolution, 5-mm slice thickness; no. of signals averaged, 8). After treatment, all rabbits were converted to normal rabbit chow (Purina Mills). In the present survival study, the postinjection imaging time point was changed from 2 to 4 hours to allow adequate recovery time from pretreatment anesthesia at baseline before the 4-hour posttreatment imaging session; this change decreased procedural morbidity and improved animal survival.[11] One week later, the level of neovascular $\alpha_v\beta_3$-integrin expression was assessed as above in all animals using integrin-targeted paramagnetic nanoparticles (1.0 mL/kg; no drug).

MRI signal enhancement from the aortic wall was averaged over all imaged slices using a custom, semiautomated segmentation program previously described.[11] Briefly, the aortic lumen was defined in each 2D image with a seeded region-growing algorithm. The aortic wall was defined by dilation of the luminal mask followed by automated thresholding to obtain a consistent and objective region-of-interest (ROI) encompassing the entire aortic wall, which was evaluated by visual inspection. A minority of the ROIs, typically 2 to 3 slices of 20, clearly extended beyond the aortic wall and was excluded from further analysis. Image intensity was normalized relative to a fiduciary marker (test tube with 25 μmol/L gadolinium diethylene-triamine-pentaacetic acid in saline) placed within the field of view. Signal enhancement in the aortic wall was measured for each individual animal using all segmented slices. The percent enhancement in the MR signal was calculated slice-by-slice in the 4-hour postinjection images relative to the average preinjection MR signal, providing an unbiased integrated measurement of contrast enhancement in the aortic wall.

Hematology and Clinical Chemistry

Blood samples were drawn from the ear vein after the 80-day high-cholesterol diet and following the last imaging session (1 week later) to assess clinical chemistries and hematology. Samples were analyzed by the Washington University Department of Comparative Medicine using routine clinical chemistry procedures.

Histology and Immunohistology

A separate cohort of cholesterol-fed rabbits was injected with $\alpha_v\beta_3$-targeted nanoparticles either with (n=4) or without (n=4) fumagillin and euthanized 1 week later for microscopic evaluation of the neovasculature. The abdominal aorta was divided into 5-mm segments from the diaphragm to 5 cm past the renal arteries, removed and frozen in Optimal Cutting Temperature medium. One 4-μm section cut from each 5-mm segment was stained for the expression of platelet endothelial cell adhesion molecule 1 (PECAM-1) (Chemicon International Inc), using routine methods previously described.[11] Microscopic images were obtained using a Nikon E800 research microscope and digitized for quantitative histological analysis with a Nikon DXM1200 camera. The number of PECAM-positive microvessels, ie, vessels containing no more than 2 endothelial cells along the diameter, in each section was compared between fumagillin treated and untreated rabbits.

Statistics

All data were statistically analyzed using general linear models and group means for significant model effects were separated using least-significant differences ($P<0.05$, JMP, SAS Inc). All numerical results are reported as mean±SEM.

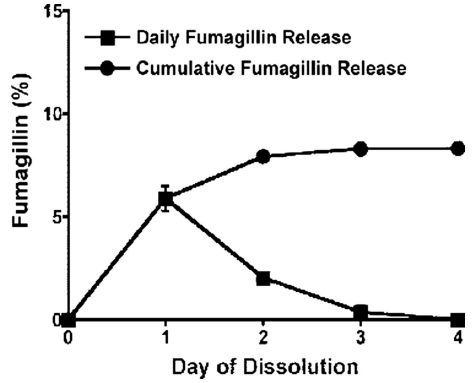

Figure 1. Daily (■) and cumulative (●) release of fumagillin from the nanoparticle membrane. The hydrophobic nature of fumagillin permits <10% to be released.

Results

Nanoparticle Characteristics

All 3 paramagnetic nanoparticle formulations (ie, $\alpha_v\beta_3$-targeted fumagillin nanoparticles, $\alpha_v\beta_3$-targeted nanoparticles without fumagillin, and nontargeted fumagillin nanoparticles) had similar particle size distributions with nominal diameters ranging from 175 to 220 nm. Paramagnetic payloads (≈90 000 gadolinium ions per particle) were similar to nanoparticle formulations previously reported.[8,11,22] Both the targeted and nontargeted fumagillin nanoparticles incorporated ≈87% of the theoretical drug payload (30 μg fumagillin per milliliter) for a net dosage of ≈26 μg/kg body weight. Because of its hydrophobic nature, fumagillin was well retained with less than 9% of the incorporated dosage diffusing from the nanoparticles under sink conditions during in vitro dissolution (Figure 1). The majority of fumagillin release in vitro occurred during the first day (≈5%) and further release was undetectable by the fourth day.

Clinical Chemistry and Hematology

Serum cholesterol levels of hyperlipidemic rabbits were 1550±160 mg/dL after 80 days of high-cholesterol diet ($\alpha_v\beta_3$-targeted fumagillin nanoparticles: 1440±220 mg/dL; $\alpha_v\beta_3$-targeted control nanoparticles: 1380±230 mg/dL; nontargeted fumagillin nanoparticles: 1790±370 mg/dL) and remained elevated for all groups at the time of euthanasia, despite conversion to normal chow 7 days earlier ($\alpha_v\beta_3$-targeted fumagillin nanoparticles: 1130±190 mg/dL; $\alpha_v\beta_3$-targeted control nanoparticles: 1450±220 mg/dL; nontargeted fumagillin nanoparticles: 1490±210 mg/dL). Individual cholesterol levels, before and after treatment and across all treatment groups, are 40 to 60 times higher than normal (30 mg/dL).[23] There was no correlation between individual cholesterol levels at the 2 time points and week-to-week changes in aortic signal contrast. One week after treatment, no animals exhibited changes in electrolytes, hepatic function, or hematology with respect to published normal ranges.[23]

Magnetic Resonance Imaging

Confirmation of the early stage of atherosclerosis in this animal model was provided by T_1-weighted black-blood

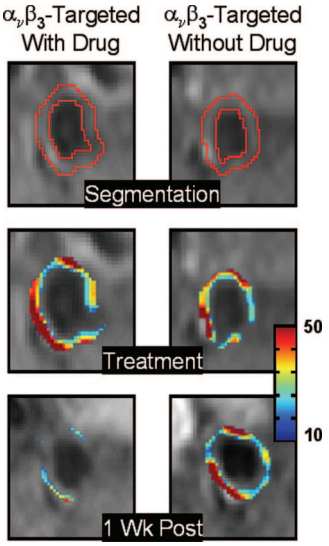

Figure 2. MRI of abdominal aorta showing outline of segmented ROI (top), false-colored overlay of percent signal enhancement at time of treatment (middle), and 1 week posttreatment (bottom). The color overlays are thresholded at 10% enhancement to show some anatomic detail within the ROI.

images that showed insignificant luminal narrowing or wall thickening as compared with age-matched, nonatherosclerotic rabbits from other studies.[11] However, even at this early stage, angiogenesis in the aortic wall was observed as MR signal enhancement following injection of $\alpha_v\beta_3$-targeted nanoparticles, both with and without fumagillin. The distribution of contrast enhancement was patchy across all imaging slices with typically higher levels of angiogenesis noted near the diaphragm (Figure 2, middle panels). Nontargeted nanoparticles (with fumagillin) produced less extensive MR enhancement of the neovasculature at much lower levels with a similarly heterogeneous distribution, consistent with previous reports.[11] The average MR signal enhancement per slice integrated across the entire aortic wall and along the entire imaged length was identical for $\alpha_v\beta_3$-targeted nanoparticles with (16.7±1.1%) and without (16.7±1.6%) fumagillin (Figure 3, black bars). Nontargeted nanoparticles, however, provided less signal enhancement (10.8±1.1%, $P<0.05$), representing delayed washout from the tortuous microvasculature.[12] Because the circulating half-life of nanoparticles is approximately

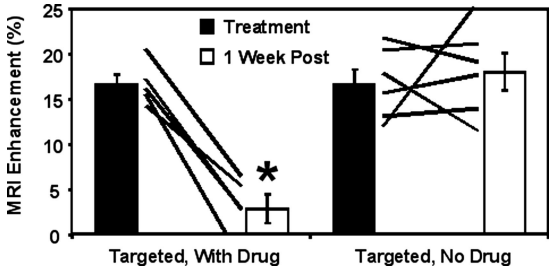

Figure 3. Aortic MRI signal enhancement averaged over all imaged slices at the time of treatment (filled bars) and 1 week after treatment (open bars). Rabbits treated with $\alpha_v\beta_3$-targeted fumagillin nanoparticles had lower angiogenesis at 1 week compared with nanoparticles without fumagillin (*$P<0.05$). The solid lines indicate individual animal response to treatment over the 7-day period.

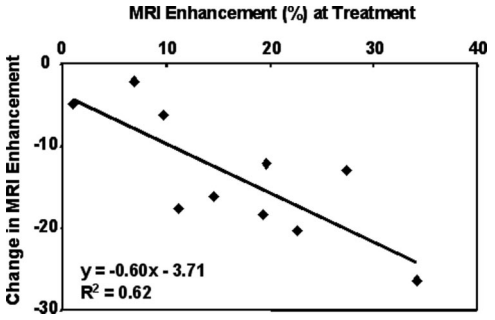

Figure 4. MRI signal enhancement at the time of treatment correlates to the change in signal 7 days after treatment. Sections of the abdominal aorta with the highest signal enhancement at the time of $\alpha_v\beta_3$-targeted fumagillin nanoparticle treatment show the greatest reduction in $\alpha_v\beta_3$-integrin expression assessed 1 week later.

300±110 minutes,[24] MRI measurements obtained at 4 hours reflect the differential rate of nanoparticle uptake and clearance, which was consistent with previous results in hyperlipidemic rabbits and numerous cancer models.[7,8,11]

One week after antiangiogenic nanoparticle treatment, the expression of $\alpha_v\beta_3$ integrin was assessed as a marker of residual neovasculature within the aortic wall. Preinjection scans were collected, followed by injection of $\alpha_v\beta_3$-targeted paramagnetic nanoparticles (without drug) and contrast enhancement imaging was performed 4 hours postinjection as outlined above. The preinjection aortic wall signal intensities for all groups at the time of treatment and at the 1 week follow-up period were identical, confirming that the targeted paramagnetic nanoparticles administered 1 week prior were no longer detectable. However, 1 week after treatment with $\alpha_v\beta_3$-targeted fumagillin nanoparticles, both the spatial distribution of image contrast (Figure 2, lower left) and the average MRI signal enhancement (2.9±1.6%; $P<0.05$; Figure 3) was markedly reduced. By comparison, MRI signal enhancement 1 week after treatment with $\alpha_v\beta_3$-targeted nanoparticles lacking fumagillin was undiminished (18.1±2.1%; Figure 2, lower right, and Figure 3).

The trends for individual animals (Figure 3, solid lines) exhibited a consistent signal reduction of 60% to 80% in all rabbits treated with $\alpha_v\beta_3$-targeted fumagillin nanoparticles. By comparison, the MRI signal increased in 4 of 6 rabbits injected with $\alpha_v\beta_3$-targeted nanoparticles lacking fumagillin, and either no change or a slight decrease in contrast was noted in the other 2 animals. Overall, the week-to-week fluctuations among individual untreated animals likely reflected biological and measurement variability. Treatment with nontargeted fumagillin nanoparticles did not significantly diminish ($P=0.26$) $\alpha_v\beta_3$-integrin levels as determined by MR signal enhancement 1 week after treatment (12.4±0.9%).

In the 5 rabbits treated with $\alpha_v\beta_3$-targeted fumagillin nanoparticles, the aortic enhancement data from each rabbit was subdivided into 2 broad anatomic regions, diaphragm (top half) and infrarenal (bottom half), and the magnitude of contrast signal detected at the time of treatment was plotted against the percentage of contrast change observed 1 week posttreatment. Aortic areas displaying high MR enhancement at the time of treatment had the largest subsequent reduction in $\alpha_v\beta_3$-targeted MR signal 1 week later (Figure 4), suggesting that combining imaging with therapy may not only confirm and quantify the local delivery of chemotherapeutics but may also provide early prognostic information relative to anticipated treatment effects.

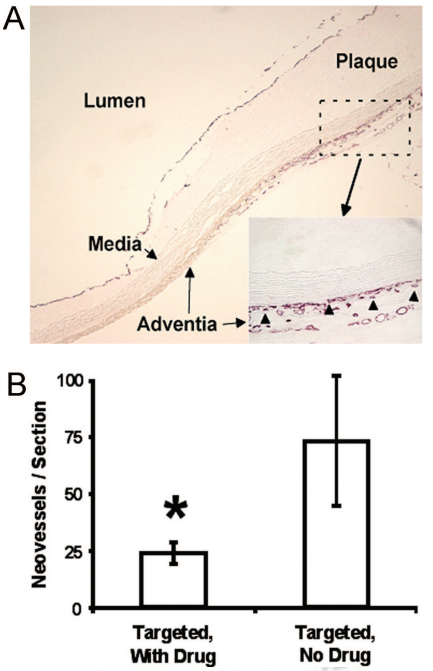

Figure 5. A, PECAM-stained section (×4) of abdominal aorta from a hyperlipidemic rabbit displaying adventitia, media and plaque. Higher magnification inset (×20) shows microvessels were predominantly located in the adventitia associated with thickening neointima. Neovessels were generally not found in regions where plaque progression was minimal or nonexistent in this cohort of rabbits. Arrowheads illustrate the type of PECAM microvessels counted within each section to assess fumagillin antiangiogenic effects. Note that larger, mature vessels positively stained for PECAM were not included in these estimates. B, The number of neovascular vessels within the adventitia was reduced (*$P=0.05$) in fumagillin-treated rabbits over the proximal half of the aorta (ie, renal artery to diaphragm), which correlated with the region of greatest MR signal and fumagillin response in the imaging studies.

Histology

In a separate cohort of animals, abdominal aorta sections obtained 1 week after nanoparticle treatment revealed mild, heterogeneously distributed intimal thickening consistent with very early atherosclerotic neointimal development in all rabbits. The majority of neovessels within the aortic wall were located in the adventitia opposite regions of thickening intimal plaque (Figure 5A). Very few vessels were observed in the media or plaque in these animals. The total number of PECAM-positive microvessels per section when averaged across all aortic slices was greater ($P=0.08$) in control rabbits receiving $\alpha_v\beta_3$-targeted particles without drug (65±28) than in those given $\alpha_v\beta_3$-targeted fumagillin nanoparticles (32±11). Histological sections from the upper half of the aorta, however, typically displayed more prominent disease and this area showed a significant difference (Figure 5B) between untreated and treated animals (73±28 versus 24±5, respectively, $P=0.05$), which paralleled the overall distribution of MR signal enhancement changes observed previously.

Discussion

The close association of angiogenesis with atherosclerotic disease and expansion of the vasa vasorum is well recognized.[25] The pathophysiological role of plaque neovascularization includes: (1) permitting plaque growth beyond a wall thickness that limits nutrient diffusion; (2) conducting inflammatory cells and lipoproteins into lesions; and (3) contributing to plaque instability and rupture.[3,26] We have recently reported specific noninvasive detection of molecular epitopes associated with angiogenesis with the use of $\alpha_v\beta_3$-targeted paramagnetic nanoparticles in hyperlipidemic New Zealand White rabbits.[11] In the present study, we extend that finding and further demonstrate that $\alpha_v\beta_3$-targeted paramagnetic nanoparticles can deliver fumagillin and elicit a marked antiangiogenic response with a minimal drug dosage. The combination of imaging and drug delivery permitted an integrated quantitative assessment of aortic neovascularity at baseline, which reflected the delivery of fumagillin nanoparticles. Reimaging with $\alpha_v\beta_3$-targeted paramagnetic nanoparticles 1 week later revealed a significant decrease in the integrated MR signal in rabbits receiving $\alpha_v\beta_3$ nanoparticles with fumagillin versus control nanoparticles. Similarly, in a second cohort of early atherosclerotic rabbits, adventitial angiogenic expansion of the vasa vasorum measured microscopically was markedly reduced after a single dose of $\alpha_v\beta_3$-targeted fumagillin nanoparticles in comparison to controls. Comparing the magnitude of MR enhancement at baseline in rabbits receiving $\alpha_v\beta_3$-nanoparticles with fumagillin with the change in contrast detected 1 week after treatment revealed an inverse relationship, suggesting that imaging data obtained at baseline was predictive of antiangiogenic changes 1 week later. Collectively, these data suggest that integrin-targeted paramagnetic nanoparticles may be useful for obtaining quantitative intramural assessments of atherosclerotic status, as reflected by a neovascular biomarker, for delivering potent antiangiogenic compounds that could stabilize or reverse plaque progression and for noninvasively assessing the intramural effectiveness of treatment.

Fumagillin was efficiently incorporated (ie, 87%) in the nanoparticle surfactant layer and highly retained during dissolution under infinite sink conditions. We have reported that effectiveness of therapeutic nanoparticles is dependent on their close and prolonged apposition with the target membrane surface caused by ligand–receptor interactions.[16] Increased collisional interactions facilitated by ligand-directed binding promote the concomitant exchange of therapeutic agents and lipids from the encapsulating monolayer to the target cell membranes. The transfer of membrane components between lipid vesicles and cell membranes has been described and initially modeled by others.[27,28] Ordinarily, collision-mediated lipid exchange proceeds as a slow, concentration-dependent, second-order process of little consequence for circulating lipid particle systems. However, the present data suggest that direct binding of fumagillin nanoparticles to $\alpha_v\beta_3$ integrin decreases the activation energy barrier for the desorption of lipid molecules to the endothelial cell membrane by minimizing the equilibrium separation of surfaces and by promoting the formation of collisional or fusional lipid complexes.[29,30] We have termed this mechanism "contact facilitated drug delivery."[16,31] By comparison, significant antineovascular effects were not observed for control $\alpha_v\beta_3$ integrin–targeted nanoparticles nor for nontargeted fumagillin nanoparticles.

The potential use of antiangiogenic therapy in atherosclerotic disease was first reported by Moulton et al in apoE$^{-/-}$ mice treated for 4 months (20 to 36 weeks) with TNP-470, a water-soluble fumagillin analogue, or endostatin (30 mg/kg every other day, 1.68 g/kg total dose).[13] Reduction in plaque angiogenesis and diminished atheroma growth were noted despite persistent elevation of total cholesterol levels. In the present study, a single administration of $\alpha_v\beta_3$-targeted fumagillin nanoparticles, at a total dosage approximately 50 000 times lower than the cumulative oral dose of TNP-470 reported previously, effectively diminished neovascular density in the adventitia as determined by MRI and immunohistochemistry. The dramatic reduction in dosage facilitated by targeted drug delivery could substantially minimize the dose-related adverse effects previously reported for TNP-470.[14]

Neovascular expansion of the vasa vasorum in atherosclerosis is stimulated and reflective of the increased metabolic demands of the expanding atheroma and provides a conduit for inflammatory cells and lipids into the plaque. Moreover, intraplaque rupture and hemorrhage of angiogenic vessels further exacerbates the inflammatory state and increases the vulnerability of the lesions.[32] Careful microscopic study of plaque neovasculature further suggests that the highest levels were associated with ruptured lesions and lipid-rich plaques, whereas the lowest microvascular densities were associated with stable, fibrocalcific lesions.[3]

Noninvasive quantification of microvascular density as a surrogate marker of atherosclerotic plaques using $\alpha_v\beta_3$-targeted paramagnetic nanoparticles integrated over small or large segments of vasculature could provide quantitative estimates of intramural disease burden and severity. In cases of rapidly advancing disease, the local delivery of potent antiangiogenic agents might acutely inhibit plaque progression and afford more opportunity for traditional therapeutic approaches, such as HMG-CoA reductase inhibitors, to provide long-term maintenance of the antineovascular effects.

Limitations

In this study, we used integrated measurements over large segments of the aortic wall to depict the overall atherosclerotic burden and the general vascular response to the antiangiogenic treatment. However, one can anticipate that developments in image acquisition and reconstruction methods, such as motion tracking, parallel imaging, and elastic registration of images, as well as the wider availability of higher field scanners (3.0 T), will likely improve overall signal-to-noise and image resolution to allow comparable measurements and serial evaluation of focal disease in all vessels, including the coronary arteries, if

clinically warranted. However, further assessments of variability introduced biologically or technically will need to be delineated and addressed as this and similar technologies develop.

Although decreased angiogenesis was observed by both MRI and immunohistochemistry 7 days after fumagillin treatment, more extensive investigation of longer follow-up intervals and different drug regimens are required to elucidate the physiological consequences for plaque stabilization or regression, likely in a different animal model. The integrated use of targeted parenteral and current chronic oral therapies will need to be studied. Likely, complimentary imaging modalities, such as 3D micro-CT, may be used to further characterize the consequences of antiangiogenic interventions.

Conclusions

In this study, we used targeted paramagnetic nanoparticles to noninvasively assess $\alpha_v\beta_3$-integrin expression in the aortic wall of hyperlipidemic rabbits during early atherosclerosis. Fumagillin, an endothelium selective antiangiogenic compound, was incorporated into the surfactant layer of the targeted MRI agent and resulted in a marked reduction of neovasculature with a single application of a drug dosage orders of magnitude less previously reported. Microscopic assessment of neovasculature changes following $\alpha_v\beta_3$-targeted fumagillin nanoparticles revealed a significant decrease in microvasculature relative to controls, which paralleled the MRI findings. We hypothesize that $\alpha_v\beta_3$-targeted particles could serve as a unique nanomedicine tool for noninvasive characterization, drug delivery, and monitoring in atherosclerosis.

Acknowledgments

We thank Ralph W. Fuhrhop for technical assistance in producing the nanoparticle formulations.

Sources of Funding

We acknowledge grant support from the National Institutes of Health (HL-78631, HL-73646, NO1-CO-37007, and EB-01704), the American Heart Association, and Philips Medical Systems.

Disclosures

None.

References

1. Gossl M, Rosol M, Malyar NM, Fitzpatrick LA, Beighley PE, Zamir M, Ritman EL. Functional anatomy and hemodynamic characteristics of vasa vasorum in the walls of porcine coronary arteries. *Anat Rec A Discov Mol Cell Evol Biol.* 2003;272:526–537.
2. Tenaglia AN, Peters KG, Sketch MH Jr, Annex BH. Neovascularization in atherectomy specimens from patients with unstable angina: implications for pathogenesis of unstable angina. *Am Heart J.* 1998; 135:10–14.
3. Moreno PR, Purushothaman KR, Fuster V, Echeverri D, Truszczynska H, Sharma SK, Badimon JJ, O'Connor WN. Plaque neovascularization is increased in ruptured atherosclerotic lesions of human aorta: implications for plaque vulnerability. *Circulation.* 2004;110: 2032–2038.
4. Khurana R, Zhuang Z, Bhardwaj S, Murakami M, De Muinck E, Yla-Herttuala S, Ferrara N, Martin JF, Zachary I, Simons M. Angiogenesis-dependent and independent phases of intimal hyperplasia. *Circulation.* 2004;110:2436–2443.
5. Kolodgie FD, Gold HK, Burke AP, Fowler DR, Kruth HS, Weber DK, Farb A, Guerrero LJ, Hayase M, Kutys R, Narula J, Finn AV, Virmani R. Intraplaque hemorrhage and progression of coronary atheroma. *N Engl J Med.* 2003;349:2316–2325.
6. Anderson SA, Rader RK, Westlin WF, Null C, Jackson D, Lanza GM, Wickline SA, Kotyk JJ. Magnetic resonance contrast enhancement of neovasculature with alpha(v)beta(3)-targeted nanoparticles. *Magn Reson Med.* 2000;44:433–439.
7. Schmieder AH, Winter PM, Caruthers SD, Harris TD, Williams TA, Allen JS, Lacy EK, Zhang H, Scott MJ, Hu G, Robertson JD, Wickline SA, Lanza GM. Molecular MR imaging of melanoma angiogenesis with alphanubeta3-targeted paramagnetic nanoparticles. *Magn Reson Med.* 2005;53:621–627.
8. Winter PM, Caruthers SD, Kassner A, Harris TD, Chinen LK, Allen JS, Lacy EK, Zhang H, Robertson JD, Wickline SA, Lanza GM. Molecular imaging of angiogenesis in nascent Vx-2 rabbit tumors using a novel alpha(nu)beta3-targeted nanoparticle and 1.5 tesla magnetic resonance imaging. *Cancer Res.* 2003;63:5838–5843.
9. Sipkins DA, Cheresh DA, Kazemi MR, Nevin LM, Bednarski MD, Li KC. Detection of tumor angiogenesis in vivo by alphaVbeta3-targeted magnetic resonance imaging. *Nat Med.* 1998;4:623–626.
10. Stupack DG, Cheresh DA. Integrins and angiogenesis. *Curr Top Dev Biol.* 2004;64:207–238.
11. Winter PM, Morawski AM, Caruthers SD, Fuhrhop RW, Zhang H, Williams TA, Allen JS, Lacy EK, Robertson JD, Lanza GM, Wickline SA. Molecular imaging of angiogenesis in early-stage atherosclerosis with alpha (v) beta3-integrin-targeted nanoparticles. *Circulation.* 2003;108:2270–2274.
12. Wilson SH, Herrmann J, Lerman LO, Holmes DR Jr, Napoli C, Ritman EL, Lerman A. Simvastatin preserves the structure of coronary adventitial vasa vasorum in experimental hypercholesterolemia independent of lipid lowering. *Circulation.* 2002;105:415–418.
13. Moulton KS, Heller E, Konerding MA, Flynn E, Palinski W, Folkman J. Angiogenesis inhibitors endostatin or TNP-470 reduce intimal neovascularization and plaque growth in apolipoprotein E-deficient mice. *Circulation.* 1999;99:1726–1732.
14. Herbst RS, Madden TL, Tran HT, Blumenschein GR Jr, Meyers CA, Seabrooke LF, Khuri FR, Puduvalli VK, Allgood V, Fritsche HA Jr, Hinton L, Newman RA, Crane EA, Fossella FV, Dordal M, Goodin T, Hong WK. Safety and pharmacokinetic effects of TNP-470, an angiogenesis inhibitor, combined with paclitaxel in patients with solid tumors: evidence for activity in non-small-cell lung cancer. *J Clin Oncol.* 2002;20:4440–4447.
15. Liu S, Widom J, Kemp CW, Crews CM, Clardy J. Structure of human methionine aminopeptidase-2 complexed with fumagillin. *Science.* 1998;282:1324–1327.
16. Lanza GM, Yu X, Winter PM, Abendschein DR, Karukstis KK, Scott MJ, Chinen LK, Fuhrhop RW, Scherrer DE, Wickline SA. Targeted antiproliferative drug delivery to vascular smooth muscle cells with a magnetic resonance imaging nanoparticle contrast agent: implications for rational therapy of restenosis. *Circulation.* 2002;106:2842–2847.
17. Harris TD, Kalogeropoulos S, Nguyen T, Liu S, Bartis J, Ellars C, Edwards S, Onthank D, Silva P, Yalamanchili P, Robinson S, Lazewatsky J, Barrett J, Bozarth J. Design, synthesis, and evaluation of radiolabeled integrin alpha v beta 3 receptor antagonists for tumor imaging and radiotherapy. *Cancer Biother Radiopharm.* 2003;18: 627–641.
18. Meoli DF, Sadeghi MM, Krassilnikova S, Bourke BN, Giordano FJ, Dione DP, Su H, Edwards DS, Liu S, Harris TD, Madri JA, Zaret BL, Sinusas AJ. Noninvasive imaging of myocardial angiogenesis following experimental myocardial infarction. *J Clin Invest.* 2004;113: 1684–1691.
19. Sadeghi MM, Krassilnikova S, Zhang J, Gharaei AA, Fassaei HR, Esmailzadeh L, Kooshkabadi A, Edwards S, Yalamanchili P, Harris TD, Sinusas AJ, Zaret BL, Bender JR. Detection of injury-induced vascular remodeling by targeting activated alphavbeta3 integrin in vivo. *Circulation.* 2004;110:84–90.
20. Flacke S, Fischer S, Scott MJ, Fuhrhop RJ, Allen JS, McLean M, Winter P, Sicard GA, Gaffney PJ, Wickline SA, Lanza GM. Novel MRI contrast agent for molecular imaging of fibrin: implications for detecting vulnerable plaques. *Circulation.* 2001;104:1280–1285.
21. Morawski AM, Winter PM, Crowder KC, Caruthers SD, Fuhrhop RW, Scott MJ, Robertson JD, Abendschein DR, Lanza GM, Wickline SA. Targeted nanoparticles for quantitative imaging of sparse molecular epitopes with MRI. *Magn Reson Med.* 2004;51:480–486.

22. Winter PM, Caruthers SD, Yu X, Song SK, Chen J, Miller B, Bulte JW, Robertson JD, Gaffney PJ, Wickline SA, Lanza GM. Improved molecular imaging contrast agent for detection of human thrombus. *Magn Reson Med.* 2003;50:411–416.
23. Olfert ED, Cross BM, McWilliam AA. *Guide to The Care and Use of Experimental Animals.* Ontario, Canada: Canadian Council on Animal Care; 1993.
24. Hu G, Lijowski M, Zhang H, Caruthers SD, Kiefer G, Gulyas G, Athey P, Harris TD, Wickline SA, Lanza GM. Molecular imaging of a_nb_3-integrin expression with targeted 111In nanoparticles in the Vx-2 rabbit tumor model. *Int J Cancer.* Submitted.
25. O'Brien ER, Garvin MR, Dev R, Stewart DK, Hinohara T, Simpson JB, Schwartz SM. Angiogenesis in human coronary atherosclerotic plaques. *Am J Pathol.* 1994;145:883–894.
26. Moulton KS. Plaque angiogenesis: its functions and regulation. *Cold Spring Harb Symp Quant Biol.* 2002;67:471–482.
27. Hernandez-Borrell J, Mas F, Puy J. A theoretical approach to describe monolayer-liposome lipid interaction. *Biophys Chem.* 1990;36:47–55.
28. Jahnig F. Lipid exchange between membranes. *Biophys J.* 1984;46: 687–694.
29. Jones JD, Thompson TE. Spontaneous phosphatidylcholine transfer by collision between vesicles at high lipid concentration. *Biochemistry.* 1989;28:129–134.
30. Jones JD, Thompson TE. Mechanism of spontaneous, concentration-dependent phospholipid transfer between bilayers. *Biochemistry.* 1990;29:1593–1600.
31. Crowder KC, Hughes MS, Marsh JN, Barbieri AM, Fuhrhop RW, Lanza GM, Wickline SA. Sonic activation of molecularly-targeted nanoparticles accelerates transmembrane lipid delivery to cancer cells through contact-mediated mechanisms: implications for enhanced local drug delivery. *Ultrasound Med Biol.* 2005;31:1693–1700.
32. Virmani R, Kolodgie FD, Burke AP, Finn AV, Gold HK, Tulenko TN, Wrenn SP, Narula J. Atherosclerotic plaque progression and vulnerability to rupture: angiogenesis as a source of intraplaque hemorrhage. *Arterioscler Thromb Vasc Biol.* 2005;25:2054–2061.